



# Ascorbic acid-assisted synthesis of cobalt ferrite ( $\text{CoFe}_2\text{O}_4$ ) hierarchical flower-like microspheres with enhanced lithium storage properties



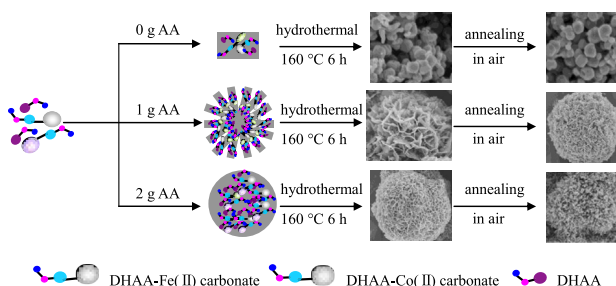
Q.Q. Xiong, J.P. Tu\*, S.J. Shi, X.Y. Liu, X.L. Wang, C.D. Gu

State Key Laboratory of Silicon Materials, Key Laboratory of Advanced Materials and Applications for Batteries of Zhejiang Province, and Department of Materials Science and Engineering, Zhejiang University, Hangzhou 310027, China

## HIGHLIGHTS

- We prepared  $\text{CoFe}_2\text{O}_4$  flower-like microspheres via a AA-assisted method.
- The microspheres are assembled by numerous porous and inter-connected lamella structures.
- The electrode shows high capacity, good cycle stability and enhanced rate performance.

## GRAPHICAL ABSTRACT



## ARTICLE INFO

### Article history:

Received 8 December 2013

Received in revised form

29 December 2013

Accepted 8 January 2014

Available online 21 January 2014

### Keywords:

Cobalt ferrite

Flower-like microspheres

Anode

Lithium ion battery

## ABSTRACT

$\text{CoFe}_2\text{O}_4$  flower-like microspheres are prepared via a surfactant- and template-free method, involving the controlled hydrothermal synthesis firstly and a subsequent thermal decomposition treatment. The microspheres with diameters of 3–4  $\mu\text{m}$  are characterized by the assembly of numerous porous and inter-connected lamella structures. Lithium-ion batteries electrodes based on the as-prepared  $\text{CoFe}_2\text{O}_4$  microspheres show a high specific capacity of 733.5  $\text{mAh g}^{-1}$  after 50 cycles at a current density of 200  $\text{mA g}^{-1}$  and a good cyclic stability, as well as excellent rate capability. The enhanced electrochemical performance can be attributed to the hierarchical microsphere structure with high sufficient interfacial contact area between the microspheres and electrolyte, the short diffusion distance of  $\text{Li}^+$ , better accommodation of structural stress and volume change with the lithiation/delithiation process. It is suggested that the  $\text{CoFe}_2\text{O}_4$  microsphere is one of the most promising candidates for high-performance lithium-ion batteries.

© 2014 Elsevier B.V. All rights reserved.

## 1. Introduction

Nowadays, with the rapid depletion of traditional fossil fuels and continually worsened environmental pollution, there is a greatly increased demand for clean and efficient energy storage devices [1]. The lithium-ion battery (LIB) is one of the most promising energy storage devices owing to its long cyclic life, high

energy density and environmental compatibility [2–9]. So as to meet the increasing need for LIBs with higher power and energy densities, researchers have paid enormous effort in devoting new electrode materials and designing novel nanostructures. Transition metal oxides as anode materials in LIBs, compared with commercial graphite (theoretical capacity 372  $\text{mAh g}^{-1}$ ), can deliver reversible lithium storage capacity of 2–3 times higher than that of commercial graphite [10–16]. Among these oxides, the ternary spinel-type oxides have shown good capacity values on cycling [17–21]. In particular, the ferrite  $\text{CoFe}_2\text{O}_4$  is promising high capacity anode material of 916  $\text{mAh g}^{-1}$  (8 mol Li per mol  $\text{CoFe}_2\text{O}_4$  can be involved

\* Corresponding author. Tel.: +86 571 87952856; fax: +86 571 87952573.

E-mail addresses: [tujp@zju.edu.cn](mailto:tujp@zju.edu.cn), [tujplab@zju.edu.cn](mailto:tujplab@zju.edu.cn) (J.P. Tu).

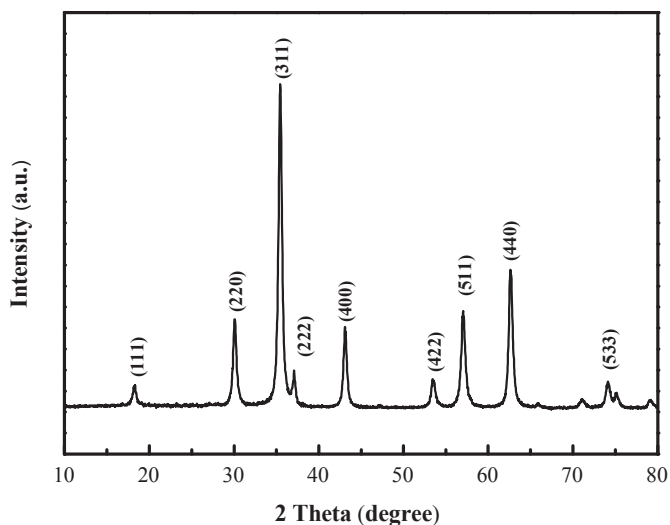


Fig. 1. XRD pattern of  $\text{CoFe}_2\text{O}_4$  flower-like microspheres.

according to the reaction  $\text{CoFe}_2\text{O}_4 + 8\text{Li}^+ + 8\text{e}^- \leftrightarrow \text{Co} + 2\text{Fe} + 4\text{Li}_2\text{O}$ , excellent chemical stability and low cost [22–25]. Despite of these attractive features,  $\text{CoFe}_2\text{O}_4$  still suffers from poor electrical conductivity and electrode pulverization arising from structural strain and large volume changes with the lithiation/delithiation process. Thus it leads to poor electrochemical performance [26]. To improve the Li storage capability, different  $\text{CoFe}_2\text{O}_4$  materials with unique structures including nanoparticles [23,27], hollow nanospheres [22], mesoporous nanospheres [28], nanorods [29] and three-dimensional ordered macroporous structure [30] have been produced. Among these works, the hollow and macroporous structure both showed a good lithium storage performance. However, they were synthesized by a time-killing process. Therefore, an emerging insight is to further optimize the electrochemical performance with easier and more energy-efficient synthesis method.

Recently, much attention has been paid to biomolecule assisted hydrothermal synthesis in the preparation of various novel inorganic materials. Because they show special structures and fascinating self-assembly functions which make them templates of unmatched type for the design and synthesis of complicated structures [31,32]. Intensive efforts have been devoted to utilizing biomolecules' special structures and strong assembling functions to

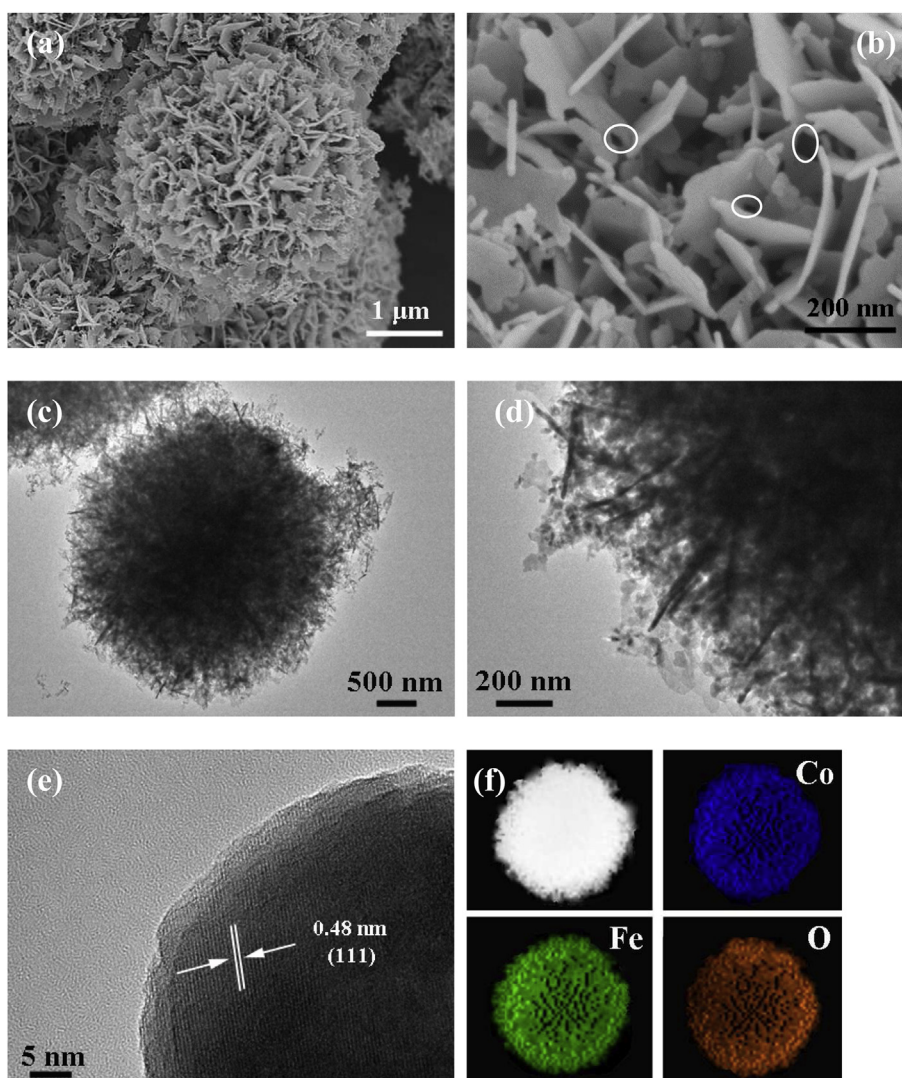


Fig. 2. SEM images (a, b) and TEM images (c, d) and HRTEM image (e) and EDS spectrum (f) of the  $\text{CoFe}_2\text{O}_4$  flower-like microspheres.

fabricate desired shapes and construct complicated superstructures in all of chemistry, biology, and materials science [33]. Ascorbic acid (AA), a small biomolecule, has been used successfully to construct complicated structures with different chemical compositions, including compound [34], metal oxides [35,36], and metals [37].

In this present work, the  $\text{CoFe}_2\text{O}_4$  flower-like microspheres were synthesized by an AA-assisted hydrothermal method. It is undoubtedly interesting in understanding the self-assembly of nanostructures and helpful to prepare functional materials. The  $\text{CoFe}_2\text{O}_4$  microspheres as the anode material for LIBs, show greatly enhanced electrochemical performance. This enhancement is mainly benefited from the sufficient contact of active material and electrolyte, the short diffusion length of  $\text{Li}^+$ , large surface area, the good accommodation of the volume expansion of active materials.

## 2. Experimental

### 2.1. Synthesis

In a typical experiment, 1.441 g  $\text{FeCl}_3 \cdot 6\text{H}_2\text{O}$ , 0.634 g  $\text{CoCl}_2 \cdot 6\text{H}_2\text{O}$ , 1 g AA ( $\text{C}_6\text{H}_8\text{O}_6$ ) and 1.2 g  $\text{CO}(\text{NH}_2)_2$  were dissolved into 80 mL deionized water under stirring to obtain a homogeneous solution. The mixture was transferred into a Teflon autoclave and was heated at 160 °C and maintained at this temperature for 6 h in an electric oven. The precipitate was collected by centrifugation and was then washed with ethanol and deionized water for several times, and was finally dried at 80 °C in an oven overnight. The product was further annealed at 500 °C for 4 h in air to obtain the  $\text{CoFe}_2\text{O}_4$  flower-like microspheres.

### 2.2. Characterization

The as-prepared samples were characterized by X-ray diffraction (XRD, Rigaku D/max 2550 PC,  $\text{Cu K}\alpha$ ), scanning electron microscopy (SEM, Hitachi S-4800 and FESEM, FEI Sirion-100), transmission electron microscopy (TEM, JEM 200CX at 160 kV, Tecnai G2 F30 at 300 kV) and X-ray photoelectron spectroscopy (XPS, Thermo ESCALAB 250Xi,  $\text{Al K}\alpha$ ).

### 2.3. Electrochemical investigation

The electrochemical tests were carried out using a coin-type half cell (CR 2025) with pure lithium metal as both the counter and reference electrodes at room temperature. The slurry consisted of a mixture of  $\text{CoFe}_2\text{O}_4$  microspheres (85 wt.%), acetylene black (10 wt.%), and polyvinylidene fluoride (PVDF) (5 wt.%), was incorporated on a piece of Cu foil ( $d = 1.5$  cm). The load weight of the  $\text{CoFe}_2\text{O}_4$  was about 2.5 mg. The electrolyte consists of 1 M  $\text{LiPF}_6$  in ethylene carbonate (EC)–dimethyl carbonate (DME) (1: 1 in volume). The polypropylene (PP) micro-porous film (Cellgard 2300) was used as a separator. The cells were assembled in an argon-filled glove box.

The galvanostatic charge–discharge cycling was performed at various current density between 0.01 and 3.0 V using a LAND battery program-control test system at room temperature ( $25 \pm 1$  °C). Cyclic voltammetry (CV) was conducted on the CHI660E electrochemical workstation at a scan rate of 0.1  $\text{mV s}^{-1}$  at 0–3.0 V (vs.  $\text{Li}^+/\text{Li}$ ). Electrochemical impedance spectroscopy (EIS) measurements were carried out in the frequency range from 100 kHz to 0.1 Hz.

## 3. Results and discussion

The cubic phase of  $\text{CoFe}_2\text{O}_4$  flower-like microspheres is obtained in Fig. 1. The XRD pattern reveals that all the reflections can be well

indexed to pure cubic  $\text{CoFe}_2\text{O}_4$  (JCPDF card No. 22-1086). Due to the sharp diffraction peaks and high intensity in the pattern, the as-prepared  $\text{CoFe}_2\text{O}_4$  can be indicated the good crystallinity. The morphology of the sample is characterized by SEM. In Fig. 2a, large scale of monodisperse hierarchical flower-like microsphere with a diameter of 3–4  $\mu\text{m}$  can be observed. The as-prepared  $\text{CoFe}_2\text{O}_4$  exhibits microsphere structure composed of numerous porous tiny lamellas and they are inter-connected (Fig. 2b). The TEM images in Fig. 2c and d further depict the microstructures of the flower-like microspheres. The HRTEM examination of the fringe of the lamella in a microsphere shown in Fig. 2e reveals a distinct set of visible lattice fringes with inter-planar spacing of 0.48 nm, corresponding to the (111) plane of  $\text{CoFe}_2\text{O}_4$ . The composition of  $\text{CoFe}_2\text{O}_4$  flower-like microspheres is also supported by the EDS elemental mapping analysis (Fig. 2f).

To investigate the chemical composition of the  $\text{CoFe}_2\text{O}_4$  flower-like microspheres, the sample is further characterized by XPS (see the Supporting Information, Fig. S1). Fig. S1a shows signals for Co, Fe, and O as well as the carbon reference. As shown in the Co 2p spectrum (Fig. S1b), a Co  $2p_{3/2}$  signal appears at 780.3 eV and its satellite peak at 786.6 eV; while Co  $2p_{1/2}$  signal and its satellite peak appear at 796.8 and 804.5 eV. As only high spin  $\text{Co}^{2+}$  cations with unpaired valence 3d electron orbitals can give rise to much stronger satellite features than low spin  $\text{Co}^{3+}$ , the Co 2p spectrum indicates Co exists in  $2^+$  oxidation state [26,38]. The Fe 2p spectrum is shown in Fig. S1c, two peaks located at 711.6 and 725.8 eV, correspond to Fe  $2p_{3/2}$  and Fe  $2p_{1/2}$ , respectively. The XPS results are in good agreement on the EDS result and the published report [39], and there are no obvious broadening peaks observed, indicating the phase-pure nature of the as-prepared  $\text{CoFe}_2\text{O}_4$  flower-like microspheres [40].

Nitrogen adsorption/desorption isotherms are measured to determine the pore size distribution and specific surface area of the  $\text{CoFe}_2\text{O}_4$  flower-like microspheres in Fig. 3. The Brunauer–Emmett–Teller (BET) surface area of the  $\text{CoFe}_2\text{O}_4$  flower-like microspheres is calculated to be  $51.0 \text{ m}^2 \text{ g}^{-1}$ , which is much higher than that of  $\text{CoFe}_2\text{O}_4$  microspheres ( $32.3 \text{ m}^2 \text{ g}^{-1}$ ) and irregular particles ( $15.1 \text{ m}^2 \text{ g}^{-1}$ ). The isotherm exhibits a hysteresis loop at the  $P/P_0$  ranges of 0.85–0.95, indicating the presence of mesopores. The pore size distribution measurement reveals that  $\text{CoFe}_2\text{O}_4$  flower-like microspheres have a dominant peak around 14.0 nm and a broad peak at 315.8 nm (Fig. 3, inset). The mesopores on the

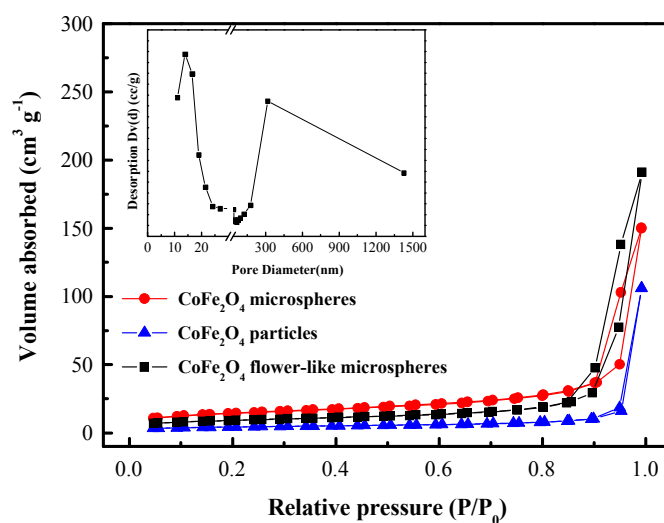
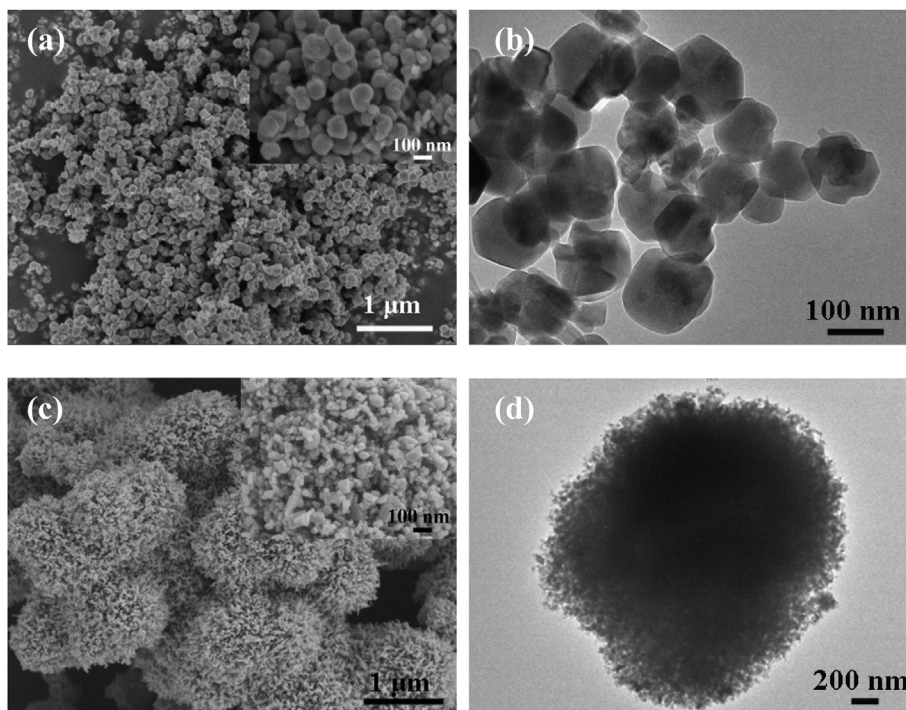


Fig. 3. Nitrogen adsorption–desorption isotherms of the  $\text{CoFe}_2\text{O}_4$  flower-like microspheres,  $\text{CoFe}_2\text{O}_4$  microspheres and irregular particles with corresponding BJH desorption pore size distributions (inset) of the  $\text{CoFe}_2\text{O}_4$  flower-like microspheres.

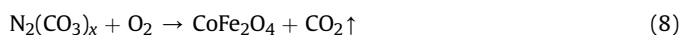
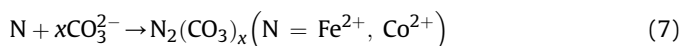
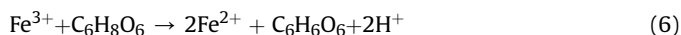
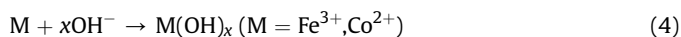
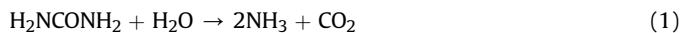


**Fig. 4.** SEM image (a) and TEM image (b) of  $\text{CoFe}_2\text{O}_4$  irregular particles with 0 g AA; SEM image (c) and TEM image (d) of  $\text{CoFe}_2\text{O}_4$  microspheres with 2 g AA.

$\text{CoFe}_2\text{O}_4$  microspheres can be attributed to the porous lamella, while the broad peak indicates the void of the constituent lamellas. The high porosity and relatively large specific surface area promote  $\text{Li}^+$  diffusion and offer large materials/electrolyte contact area [41–43].

We study the effect of amount of AA on the structure of the  $\text{CoFe}_2\text{O}_4$  as shown in Fig. 4. In the absence of AA, only  $\text{CoFe}_2\text{O}_4$  irregular particles with diameters about 50–100 nm are formed (Fig. 4a and b). When 2 g AA is added into the system, the sample is a large scale of microspheres with diameters of 1–2  $\mu\text{m}$  (Fig. 4c). In addition, it can be observed that the  $\text{CoFe}_2\text{O}_4$  microspheres are built up of many particles with sizes of 30–50 nm. TEM analysis confirms a solid interior consisting of the dense packed nanoparticle sub-units (Fig. 4d).

In order to explain the formation mechanism, we tested the products after the hydrothermal reaction by XRD (Fig. 5). Without AA, only  $\text{CoFe}_2\text{O}_4$  was formed (Fig. 5a) as follows (Eqs. (4) and (5)).



With addition of AA, by comparison with  $\text{FeCO}_3$  and  $\text{CoCO}_3$ , all the diffraction peaks could be indexed on the basis of the hexagonal phase with the space group  $R\bar{3}c$  (no. 167). In the structure, iron and cobalt occupy the octahedral sites randomly, but proportionally (Fig. 5b). We proposed the formation mechanism for the three  $\text{CoFe}_2\text{O}_4$  with different morphologies as described in Fig. 6. The reduction of Fe (III) to Fe (II) is controlled by the addition of AA as Eq. (6), which acts as the reducing agent by oxidizing its C=C double bond. With the addition of AA, the pH value decreases due to the generated  $\text{H}^+$ , then the Fe (II) and Co (II) carbonate is formed as Eq. (7). More strikingly AA's oxidized product (dehydro-ascorbic acid, DHAA) also acts as a stabilizer and capping ligand due to the chemical interaction of its carbonyl groups [44–46]. The as-produced Fe (II) and Co (II) carbonate is prone to be capped by DHAA formed in the solutions. The chemical interaction in the present system acts as an “adhesive” to facilitate the self-assembly of Fe (II) and Co (II) carbonate, which results in the different morphologies of the precursors. It is known that the carbonate ions have planar structure [35]. Then the generated Fe (II) and Co (II) carbonate tends to grow in lamellar structure. Finally the lamellar structure self-assembles through oriented attachment mechanism during the hydrothermal process [47]. It is understandable that the concentration of the as-produced organic components in the solution directly affects their self-assembly state because the interactions among them strengthen with their increased concentrations. In the absence of AA, only irregular particles are formed. In the solution with 1 g AA, the lamellar structure assembles into flower-like microspheres. When the amount of AA was increased to 2 g, DHAA–Fe (II) and DHAA–Co (II) carbonate assemble into the microspheres due to their high concentration and the strong interaction among them in the solution. Consequently, the precursors with different assemblies are formed in the solutions due to different concentrations of AA. After annealing in air, Fe (II) is oxidized to Fe (III) by oxygen in air as Eq. (8), and corresponding different morphologies of  $\text{CoFe}_2\text{O}_4$ , including irregular particles, flower-like microspheres, microspheres of nanoparticles are produced.

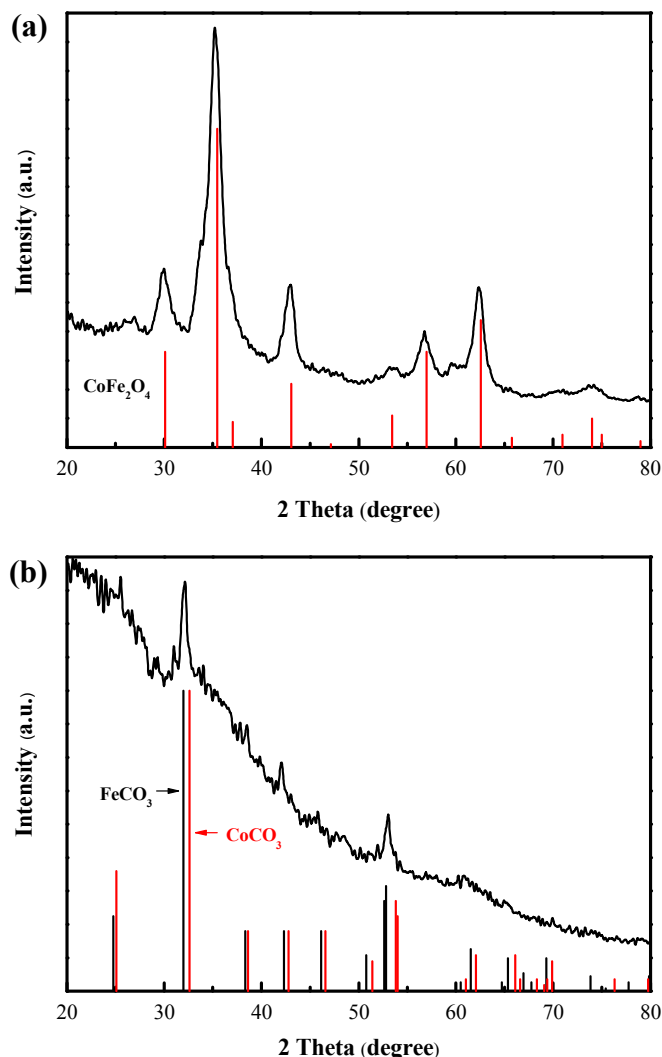


Fig. 5. XRD patterns of precursors: (a) without AA; (b) with 1 g AA.

We investigated their ability to reversibly insert/release Li<sup>+</sup> of CoFe<sub>2</sub>O<sub>4</sub> flower-like microspheres as an anode in LIBs. Fig. 7a shows the CV curves of CoFe<sub>2</sub>O<sub>4</sub> flower-like microspheres for the first three cycles in the potential range from 0 to 3.0 V (vs. Li/Li<sup>+</sup>) at a scan rate of 0.1 mV s<sup>−1</sup>. There is a big difference in the CV profiles between the first discharge process and the subsequent cycles. In

the first cycle, a sharp reduction peak appears at 0.44 V, which disappears and becomes two peaks in the subsequent cycles. The sharp reduction peak observed in the first cathodic scan is attributed to the reduction of Fe<sup>3+</sup> and Co<sup>2+</sup> to their metallic states, the formation of Li<sub>2</sub>O and the irreversible reaction with electrolyte to form a solid electrolyte interphase (SEI) film. In the second scan, two cathodic peaks appearing at 0.83 V and 1.45 V can be attributed to the reduction of Fe<sup>3+</sup> and Co<sup>2+</sup> to metallic Fe<sup>0</sup> and Co<sup>0</sup>, respectively [22]. The anodic peak at 1.75 V is observed at the first cycle, corresponding to the reversible oxidation of the Fe<sup>0</sup> and Co<sup>0</sup> to Fe<sup>3+</sup> and Co<sup>2+</sup>, respectively, which slightly shifts to a little higher potential [22,30,48]. The decrease of the individual peak intensities and integrated areas between the first cycle and the subsequent scans implies the irreversible capacity loss in the initial lithiation–delithiation process [22,49,50]. However, the integrated area and peak intensity during the cathodic and anodic process don't decrease almost in the subsequent scans, indicating the good capacity retention of the CoFe<sub>2</sub>O<sub>4</sub> flower-like microsphere electrode. Fig. 7b shows the galvanostatic charge–discharge curve for the CoFe<sub>2</sub>O<sub>4</sub> flower-like microspheres between 0.01 and 3.0 V at a current density of 200 mA g<sup>−1</sup>. Discharge curve in the first cycle consists of a sharp slope in the initial stage of the curve, a flat voltage plateau at about 0.80 V, and a long slope until 0.01 V. When discharged to 0.01 V, the initial discharge capacity of the CoFe<sub>2</sub>O<sub>4</sub> flower-like microsphere electrode is 1179.0 mAh g<sup>−1</sup>, which is larger than theoretic capacity. It comes from the formation of SEI film and possibly interfacial Li<sup>+</sup> storage during the first discharge process [12,51–52]. The second discharge curve is different from the first, suggesting drastic, Li<sup>+</sup>-driven, structural or textural modifications [12,41,53]. This charge–discharge curve is in agreement with the result found in CV measurements. Fig. 7c shows the cyclability of the CoFe<sub>2</sub>O<sub>4</sub> flower-like microspheres, CoFe<sub>2</sub>O<sub>4</sub> microspheres and irregular particles at a current density of 200 mA g<sup>−1</sup>. The specific reversible capacity of CoFe<sub>2</sub>O<sub>4</sub> flower-like microspheres after 50 cycles is 733.5 mAh g<sup>−1</sup>, much higher than those of CoFe<sub>2</sub>O<sub>4</sub> microspheres (616.7 mAh g<sup>−1</sup>) and irregular particles (427.5 mAh g<sup>−1</sup>). In addition, the CoFe<sub>2</sub>O<sub>4</sub> flower-like microspheres exhibit better capacity retention. After 50 cycles, the CoFe<sub>2</sub>O<sub>4</sub> flower-like microspheres could sustain 77.9% capacity of the 2nd cycle, compared with 65.4% for the CoFe<sub>2</sub>O<sub>4</sub> microspheres and 43.6% for the CoFe<sub>2</sub>O<sub>4</sub> irregular particles, which is attributed to its hierarchical flower-like microsphere structure with the large specific surface area to facilitate the Li ion and electron transportation. And the flower-like microspheres could also buffer the volume expansion. The cycling response at different current density is also investigated (Fig. 7d). When the current densities increase from 100 mA g<sup>−1</sup> to 2000 mA g<sup>−1</sup>, a gradual attenuation of the discharge

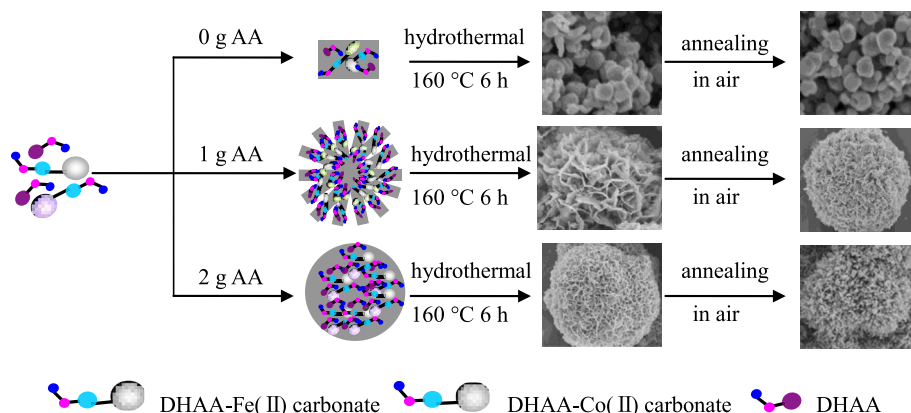
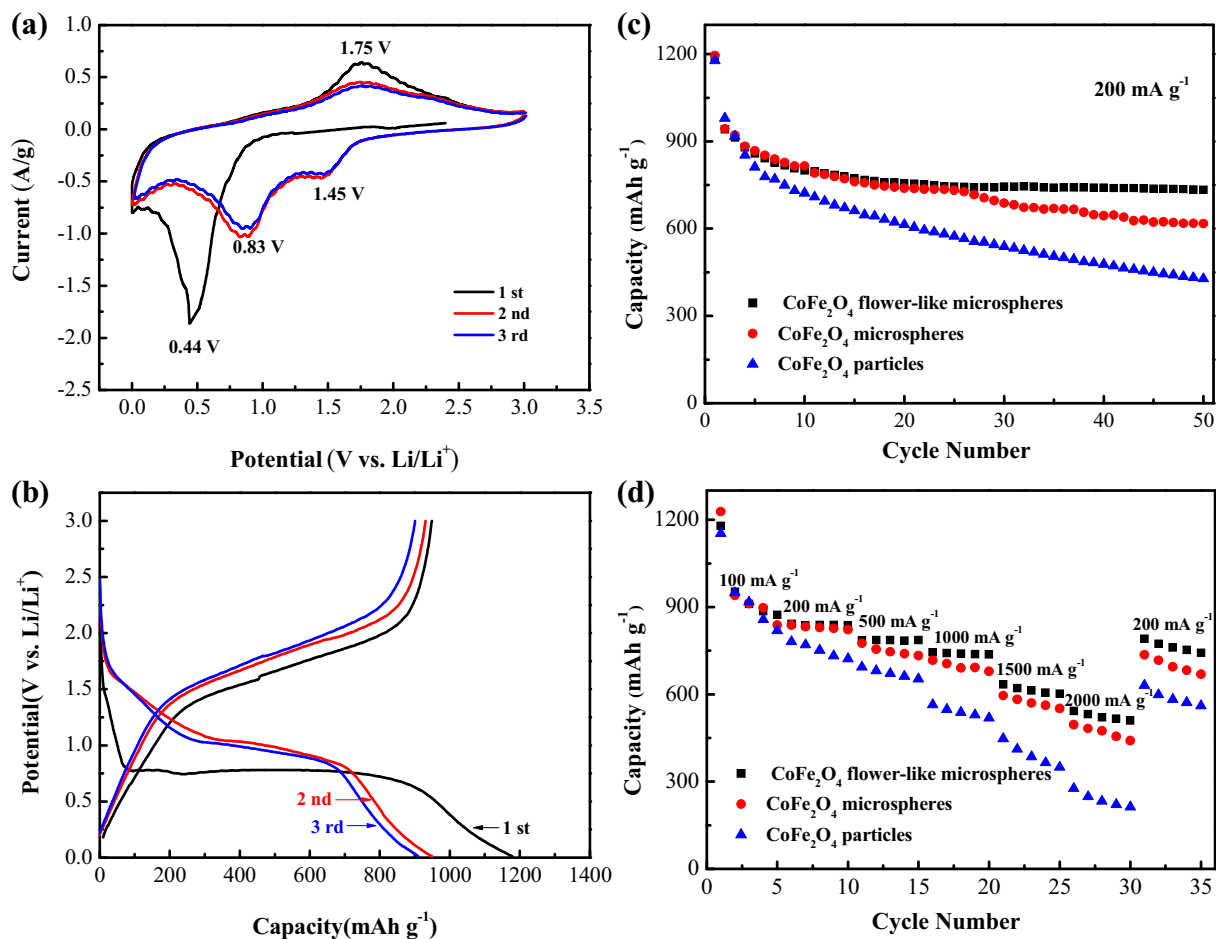


Fig. 6. Schematic diagram of the formation of the three CoFe<sub>2</sub>O<sub>4</sub> samples with different morphologies.



**Fig. 7.** (a) CV curves of  $\text{CoFe}_2\text{O}_4$  flower-like microspheres for the first three cycles at a scan rate of  $0.1 \text{ mV s}^{-1}$  in the potential range of 0–3.0 V (versus  $\text{Li/Li}^+$ ); (b) charge–discharge profiles of  $\text{CoFe}_2\text{O}_4$  flower-like microspheres between 0.01 and 3.0 V at a current density of  $200 \text{ mA g}^{-1}$ ; (c) Cycling performance of the  $\text{CoFe}_2\text{O}_4$  flower-like microspheres,  $\text{CoFe}_2\text{O}_4$  microspheres and irregular particles electrodes at a current density of  $200 \text{ mA g}^{-1}$ ; (d) Rate performance of the  $\text{CoFe}_2\text{O}_4$  flower-like microspheres,  $\text{CoFe}_2\text{O}_4$  microspheres and irregular particles electrodes at current density of  $100 \text{ mA g}^{-1}$ – $2000 \text{ mA g}^{-1}$ .

capacities for the three electrodes is observed, which may indicate that the electrode reaction is controlled by the diffusion kinetics process [53]. However, discharge capacity of  $744.1 \text{ mAh g}^{-1}$  is still maintained for the  $\text{CoFe}_2\text{O}_4$  flower-like microspheres at a current density of  $1000 \text{ mA g}^{-1}$ . Those of the  $\text{CoFe}_2\text{O}_4$  microspheres and  $\text{CoFe}_2\text{O}_4$  irregular particles drop dramatically to only  $717.0 \text{ mAh g}^{-1}$  and  $564.3 \text{ mAh g}^{-1}$ , respectively. It should be noted that when the current rate is decreased to  $200 \text{ mA g}^{-1}$ , a high discharge capacity of  $790.5 \text{ mAh g}^{-1}$  can be regained, indicating the good reversibility of the  $\text{CoFe}_2\text{O}_4$  flower-like microspheres. To the best of our knowledge,  $\text{CoFe}_2\text{O}_4$  synthesized in this experiment without any modification by other conductive materials shows better electrochemical performance than those in the published works [28,30,54]. The enhanced cycling performance and rate capability can be attributed to a more efficient transportation of Li ion and facile penetration of electrolyte in the LIBs.

The EIS test was carried out to further understand the advantage of the  $\text{CoFe}_2\text{O}_4$  flower-like microsphere electrode. Fig. 8 shows the Nyquist plots of the  $\text{CoFe}_2\text{O}_4$  flower-like microspheres,  $\text{CoFe}_2\text{O}_4$  microspheres and irregular particles electrodes after 10 cycles at a current density of  $200 \text{ mA g}^{-1}$  at the fully charged state. They have the same shapes of Nyquist plots, composed of a depressed semi-circle where a high-frequency semicircle and a medium-frequency semicircle overlap each other and a long low-frequency subsequent  $45^\circ$  line [55]. In this experiment, a modified two-parallel diffusion

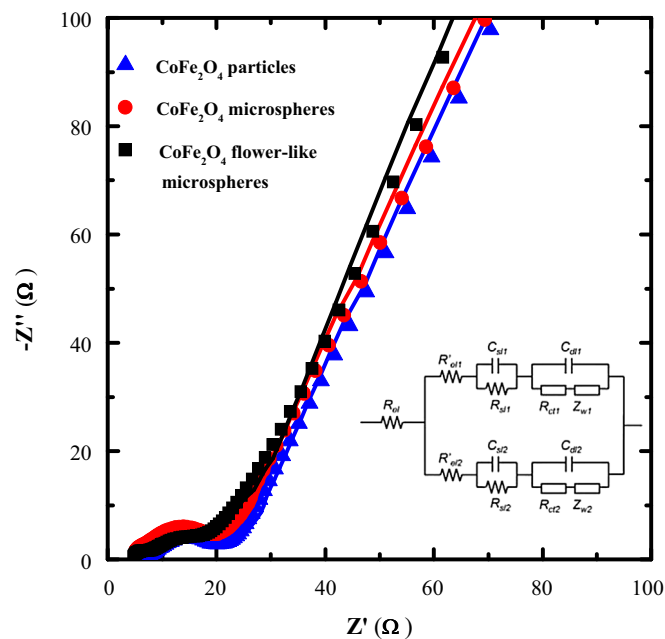


**Fig. 8.** Nyquist plots of the  $\text{CoFe}_2\text{O}_4$  flower-like microspheres,  $\text{CoFe}_2\text{O}_4$  microspheres and irregular particles electrodes after 10 cycles in the frequency range from 100 kHz to 10 mHz. The inset is the equivalent circuit.

path model is used to analyze the impedance data, and the corresponding equivalent circuit is shown in inset, where  $R_{el}$  indicates the solution impedance of cell;  $R_{sl}(i)$  and  $C_{sl}(i)$  stand for the impedance of  $Li^+$  diffusion and capacity in the surface-passivating layer, respectively;  $R_{ct}(i)$  and  $C_{dl}(i)$  designate the charge transfer impedance and double-layer capacitance at the electrode/electrolyte interface, respectively; and  $Z_W(i)$  represents the diffusion-controlled Warburg impedance ( $i = 1, 2$ ) [55,56]. The continuous lines represent the fitted spectra while the symbols are the experimental data. For the  $CoFe_2O_4$  flower-like microsphere electrode, the diameter of the semicircle, reflecting the  $R_{ct}$ , is obviously the smallest. This result as we expected indicates that the flower-like microsphere electrode has a good electronic wetting between active materials and thus a rapid charge transfer reaction during the Li insertion and extraction [11]. The curve fitting further confirms the assumption. It exhibits that the impedance of  $R_{ct}$  is  $23.2 \Omega$  for the  $CoFe_2O_4$  irregular particles,  $22.1 \Omega$  for the  $CoFe_2O_4$  microsphere, whereas it is  $18.9 \Omega$  for the  $CoFe_2O_4$  flower-like microsphere electrode.

#### 4. Conclusions

In summary, we report a controlled AA-assisted hydrothermal process and subsequent annealing at  $500^\circ C$  for 4 h in air to fabricate  $CoFe_2O_4$  flower-like microspheres in large scale. The  $CoFe_2O_4$  flower-like microspheres show high discharge capacity, good cycle performance ( $733.5 \text{ mAh g}^{-1}$  at a current density of  $200 \text{ mA g}^{-1}$  after 50 cycles), and enhanced rate capability, making it one of the most promising anode materials for high-performance LIBs. The enhanced electrochemical performance can be attributed to the hierarchical flower-like structure, which has the high interfacial contact area and good accommodation of volume change.

#### Acknowledgments

This work is supported by the Program for Innovative Research Team in University of Ministry of Education of China (IRT13037) and Key Science and Technology Innovation Team of Zhejiang Province (2010R50013). The assistances of Mr. Xin-ting Cong for SEM and TEM analysis are grateful acknowledged.

#### Appendix A. Supplementary data

Supplementary data related to this article can be found at <http://dx.doi.org/10.1016/j.jpowsour.2014.01.038>.

#### References

- [1] Q. Zhang, Y. Zhang, X.R. Wang, T. Ma, Z.B. Yuan, *Ceram. Int.* 38 (2012) 4765–4770.
- [2] J.M. Tarascon, M. Armand, *Nature* 414 (2001) 359–367.
- [3] A.S. Arico, P. Bruce, B. Scrosati, J.M. Tarascon, W. Van Schalkwijk, *Nat. Mater.* 4 (2005) 366–377.
- [4] M. Armand, J.M. Tarascon, *Nature* 451 (2008) 652–657.
- [5] M.V. Reddy, C. Yu, J.H. Fan, K.P. Loh, B.V.R. Chowdari, *ACS Appl. Mater. Interfaces* 5 (2013) 4361–4366.
- [6] X.H. Huang, J.P. Tu, X.H. Xia, X.L. Wang, J.Y. Xiang, L. Zhang, *J. Power Sources* 195 (2010) 1207–1210.
- [7] B.-Y. Jung, H.-S. Lim, Y.-K. Sun, K.-D. Suh, *J. Power Sources* 244 (2013) 177–182.
- [8] Y. Lu, J.P. Tu, Q.Q. Xiong, J.Y. Xiang, Y.J. Mai, J. Zhang, Y.Q. Qiao, X.L. Wang, C.D. Gu, S.X. Mao, *Adv. Funct. Mater.* 22 (2012) 3927–3935.
- [9] C.T. Cherian, M.V. Reddy, S.C. Haur, B.V.R. Chowdari, *ACS Appl. Mater. Interfaces* 5 (2013) 918–923.
- [10] A.K. Rai, L.T. Anh, J. Gim, V. Mathew, J. Kang, B.J. Paul, N.K. Singh, J. Song, J. Kim, *J. Power Sources* 244 (2013) 435–441.
- [11] Y.J. Mai, X.H. Xia, R. Chen, C.D. Gu, X.L. Wang, J.P. Tu, *Electrochim. Acta* 67 (2012) 73–78.
- [12] Y.J. Mai, D. Zhang, Y.Q. Qiao, C.D. Gu, X.L. Wang, J.P. Tu, *J. Power Sources* 216 (2012) 201–207.
- [13] A. Brandt, A. Balducci, *J. Power Sources* 230 (2013) 44–49.
- [14] J. Chen, X.H. Xia, J.P. Tu, Q.Q. Xiong, Y.X. Yu, X.L. Wang, C.D. Gu, *J. Mater. Chem.* 22 (2012) 15056–15061.
- [15] Y.F. Wang, L.J. Zhan, *J. Power Sources* 209 (2012) 20–29.
- [16] Q.Q. Xiong, X.H. Xia, J.P. Tu, J. Chen, Y.Q. Zhang, D. Zhou, C.D. Gu, X.L. Wang, *J. Power Sources* 240 (2013) 344–350.
- [17] R. Tummala, R.K. Guduru, P.S. Mohanty, *J. Power Sources* 199 (2012) 270–277.
- [18] J. Liu, C.P. Liu, Y.L. Wan, W. Liu, Z.S. Ma, S.M. Ji, J.B. Wang, Y.C. Zhou, P. Hodgson, Y.C. Li, *CrystEngComm* 15 (2013) 1578–1585.
- [19] L.L. Hu, B.H. Qu, C.C. Li, Y.J. Chen, L. Mei, D.N. Lei, L.B. Chen, Q.H. Li, T.H. Wang, *J. Mater. Chem. A* 18 (2013) 5596–5602.
- [20] C.W. Lee, S.D. Seo, D.W. Kim, S. Park, K. Jin, K.S. Hong, *Nano Res.* 6 (2013) 348–355.
- [21] P.F. Teh, Y. Sharma, Y.W. Ko, S.S. Pramana, M. Srinivasan, *RSC Adv.* 8 (2013) 2812–2821.
- [22] Y. Wang, D.W. Su, A. Ung, J.H. Ahn, G.X. Wang, *Nanotechnology* 23 (2012). No. 055402.
- [23] Y.H. Jin, S.D. Seo, H.W. Shim, K.S. Park, D.W. Kim, *Nanotechnology* 23 (2012). No. 125402.
- [24] S.Y. Liu, J. Xie, C.C. Fang, G.S. Cao, T.J. Zhu, X.B. Zhao, *J. Mater. Chem.* 22 (2012) 19738–19743.
- [25] Y. Ding, Y.F. Yang, H.X. Shao, *Solid State Ionics* 217 (2012) 27–33.
- [26] H. Xia, D.D. Zhu, Y.S. Fu, X. Wang, *Electrochim. Acta* 83 (2012) 166–174.
- [27] Y. Zhao, J.X. Li, Y.H. Ding, L.H. Guan, *J. Mater. Chem.* 21 (2011) 19101–19105.
- [28] Z.L. Zhang, Y.H. Wang, M.J. Zhang, Q.Q. Tan, X. Lv, Z.Y. Zhong, F.B. Su, *J. Mater. Chem. A* 1 (2013) 7444–7450.
- [29] N.N. Wang, H.Y. Xu, L. Chen, X. Gu, J. Yang, Y.T. Qian, *J. Power Sources* 247 (2014) 163–169.
- [30] Z.H. Li, T.P. Zhao, X.Y. Zhan, D.S. Gao, Q.Z. Xiao, G.T. Lei, *Electrochim. Acta* 55 (2010) 4594–4598.
- [31] W.D. Shi, S.Y. Song, H. Zhang, *Chem. Soc. Rev.* 42 (2013) 5714–5743.
- [32] Q.Y. Lu, F. Gao, S. Komarneni, *J. Am. Chem. Soc.* 126 (2004) 8650–8651.
- [33] B.X. Li, Y. Xie, Y. Xue, *J. Phys. Chem. C* 111 (2007) 12181–12187.
- [34] X.Y. Tan, J. Zhou, Q. Yang, *CrystEngComm* 13 (2011) 2792–2798.
- [35] G. Liu, Q. Deng, H.Q. Wang, D.H.L. Ng, M.G. Kong, W.P. Cai, G.Z. Wang, *J. Mater. Chem.* 22 (2012) 9704–9713.
- [36] H.T. Ren, S.Y. Jia, S.H. Wu, Y. Liu, X. Han, *Mater. Lett.* 101 (2013) 69–71.
- [37] M. Iliut, C. Leordean, V. Canpean, C.M. Teodorescu, S. Astilean, *J. Mater. Chem. C* 1 (2013) 4094–4104.
- [38] N.W. Li, M.B. Zheng, X.F. Chang, G.B. Ji, H.L. Lu, L.P. Xue, L.J. Pan, J.M. Cao, *J. Solid State Chem.* 184 (2011) 953–958.
- [39] T. Bala, C.R. Sankar, M. Baidakova, V. Osipov, T. Enoki, P.A. Joy, B.L.V. Prasad, M. Sastry, *Langmuir* 21 (2005) 10638–10643.
- [40] Y.D. Meng, D.R. Chen, X.L. Jiao, *Eur. J. Inorg. Chem.* 25 (2008) 4019–4023.
- [41] P. Poizot, S. Laruelle, S. Grugeon, L. Dupont, J.M. Tarascon, *Nature* 407 (2000) 496–499.
- [42] P.G. Bruce, B. Scrosati, J.M. Tarascon, *Angew. Chem. Int. Ed.* 47 (2008) 2930–2946.
- [43] Q.Q. Xiong, J.P. Tu, Y. Lu, J. Chen, Y.X. Yu, Y.Q. Qiao, X.L. Wang, C.D. Gu, *J. Phys. Chem. C* 116 (2012) 6495–6502.
- [44] Z. Li, L. Wei, M.Y. Gao, H. Lei, *Adv. Mater.* 17 (2005) 1001–1005.
- [45] Z. Li, H. Chen, H.B. Bao, M.Y. Gao, *Chem. Mater.* 16 (2004) 1391–1393.
- [46] L. Xiao, J. Li, D.F. Brougham, E.K. Fox, N. Feliu, A. Bushmelev, A. Schmidt, N. Mertens, F. Kiessling, M. Valldor, B. Fadeel, S. Mathur, *ACS Nano* 5 (2011) 6315–6324.
- [47] L.P. Zhu, H.M. Xiao, X.M. Liu, S.Y. Fu, *J. Mater. Chem.* 16 (2006) 1794–1797.
- [48] P. Lavela, J.L. Tirado, M. Womes, J.C. Jumas, *J. Electrochem. Soc.* 156 (2009) 589–A594.
- [49] Y.Q. Chu, Z.W. Fu, Q.Z. Qin, *Electrochim. Acta* 49 (2004) 4915–4921.
- [50] Y. Wang, D.W. Su, C.Y. Wang, G.X. Wang, *Electrochem. Commun.* 29 (2013) 8–11.
- [51] A. Debart, L. Dupont, P. Poizot, J.B. Leriche, J.M. Tarascon, *J. Electrochem. Soc.* 148 (2001) A1266–A1274.
- [52] Q.Q. Xiong, J.P. Tu, Y. Lu, J. Chen, Y.X. Yu, X.L. Wang, C.D. Gu, *J. Mater. Chem.* 22 (2012) 18639–18645.
- [53] C. Montella, *J. Electroanal. Chem.* 518 (2002) 61–83.
- [54] Y.N. Nuli, Q.Z. Qin, *J. Power Sources* 142 (2005) 292–297.
- [55] J.Y. Xiang, J.P. Tu, Y.Q. Qiao, X.L. Wang, J. Zhong, D. Zhang, C.D. Gu, *J. Phys. Chem. C* 115 (2011) 2505–2513.
- [56] J.Y. Xiang, X.L. Wang, J. Zhong, D. Zhang, J.P. Tu, *J. Power Sources* 196 (2011) 379–385.